Computer Assisted Mechanics and Engineering Sciences, 8: 609–628, 2001.

Non-constant coefficient friction models in 3d simulation of drawing processes

Jacek Rońda[1] and Kevin W. Colville
Western Cape Welding Research Group, University of Cape Town, Rondebosch, 7701 South Africa

Oskar Mahrenholtz
Technische Universität Hamburg-Harburg, Offshore Section II, Eissendorfer Str. 42, 21071 Hamburg, Germany

(Received November 3, 2000)

Different friction models: the classic one proposed by Amontons–Coulomb (AC) with a constant friction coefficient, a three-parameter model proposed by Wriggers et al. [9], and a model based on the concept of 'work-hardening' proposed by de Souza Neto et al. [8], are applied to the 3-D square-cup drawing and S-rail stamping FE simulations. The benchmark problems used during NUMISHEET'93 for a cup drawing and NUMISHEET'96 for S-rail stamping were simulated here. The results obtained for these three models are presented to illustrate the influence of the friction model on the drawing process.

NOTATION

n_I	unit normal at contact point
p_I	surface traction
p_{N}	contact pressure
$p_{\mathrm{T}I}$, p_α	friction stress vector
S_{IJ}	2nd Piola-Kirchoff stress tensor
u_I	displacement in Lagrangian frame
u_{N}	displacement normal to surface
$u_{\mathrm{T}I}$, u_α	displacement in contact plane = frictional sliding
$\dot{u}_\alpha$	rate of frictional sliding
$\dot{u}_\alpha^{\mathrm{ad}}$	rate of elastic adhesive state sliding
$\dot{u}_\alpha^{\mathrm{sl}}$	rate of frictional slip (non-recoverable sliding)
k_{T}	tangential contact stiffness constant
γ	magnitude of slip
Ψ	slip potential function
Φ	slip yield function
μ	coefficient of friction (c.o.f.)
α, β, ν	parameters of the WVS model
ω	density of frictional work
$\mu(\omega)$	friction function of WH model
δ_{IJ}	identity tensor
ρ_0	density of material at $t = 0$
$\rho_0 t_I$	body forces

[1]Corresponding author (email: ronda@maths.uct.ac.za); on leave from Warsaw University of Technology.

$\rho_0 f_I$	inertia forces
E_{IJ}	Green-Lagrange strain
$\mathbf{L}^{\mathrm{EP}}_{KLMN}$	elastic-plastic hyper-operator
${}^t\Omega$	body at time t
${}^t\Gamma$	surface of body at time t
${}^t\Gamma_U$	surface subject to displacement boundary conditions
$\phi(\mathbf{X}, t)$	prescribed displacement boundary condition
${}^t\Gamma_F$	surface subject to force boundary conditions
G_I	prescribed force boundary condition
${}^t\Gamma_C$	contact surface subject to friction
T_{T_i}	frictional stress, also p_α
ε	strain

1. Introduction

The purpose of this paper is to compare three different friction models in the finite element method (FEM) simulation of a complex metal-forming processs. The process chosen is prismatic square-cup deep-drawing as proposed for the NUMISHEET'93 conference, and the S-rail stamping simulation chosen for the NUMISHEET'96 conference. As a result of the conference data is available against which to compare the results of the simulations, and also a very detailed standard set of data is available describing the simulations.

Three different friction models are used: the classic Amontons–Coulomb model with a constant coefficient of friction, a nonlinear model proposed by Wriggers, vu Van and Stein [9] which uses three constant parameters (WVS), and a model proposed by de Souza Neto et al. [8] which is based upon work-hardening (WH). This model is appropriate for coated sheet metal, and takes into consideration wear of the surface coating.

The foundation for the friction model is based upon that proposed by Michałowski and Mróz [4] and the work of Curnier [1]. The three models, AC, WVS, WH, are modifications of the basic model where the relationship between frictional limit stress and contact pressure is varied taking into account material behavour and experimental data.

All three friction models presented here are static and do not consider the kinetics of blank motion around punch and die roundings, where normals rotate through almost 90°, which affects particle velocity. The kinetic effects of rotation are considered in a co-rotational model [6].

The simulation is implemented in the finite element program PAM-Stamp, released by PAM-System International of France. That programm is well known in automotive industry and impemented by all leading car designers. Finite strain shell elements and user friction routines are used here for stamping simulation. The material model used is elastic-plastic with hardening, with the given relation between yield stress and plastic strain as was provided by the NUMISHEET experimental data. The symmetry of the square-cup deep-drawing process allows one-quarter of the process to be used in the simulation. The tools: die, stamp, and blankholder, are modelled using rigid Bézier surfaces. The blank is modelled using the shell elements described. All tools dimensions, process parameters and material properties are approved by the automotive industries. The S-rail simulation has no symmetry and the entire tool set has to be used.

The results for major and minor strains, and also contour maps of thickness changes, for the two simulations with various friction models are presented and discussed.

2. Friction models

Introducing the concept of a slip rule Ψ and a slip criterion Φ the three friction models considered: the standard classical Amontons-Coulomb (AC) model, a model proposed by Wriggers, vu Van and

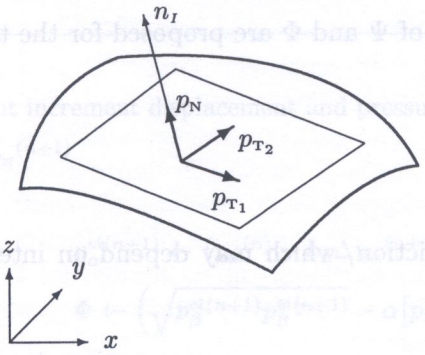

Fig. 1. The local directions for the friction variables at the contact point

Stein [9] (WVS), and a work-hardening (WH) model proposed by de Souza Neto, et al. [8], can be shown to be based on the same rules. These rules are the following:

- the decomposition of the surface traction (stress vector) $p_I = S_{IJ}n_J$ into:
  - the normal component $p_N = S_{IJ}n_In_J$,
  - and the tangential component $p_{TI} = p_I - p_N n_I$,

  as can be seen in Fig. 1,
- the decomposition of the relative displacement at the contact surface u_I into:
  - the normal component $u_N = u_I n_I$,
  - and the tangential component $u_{TI} = u_I - u_N n_I$,
- the decomposition of the rate of tangential displacement $\dot{u}_\alpha = \dot{u}_\alpha^{ad} + \dot{u}_\alpha^{sl}$ that can be also expressed by increments $\Delta u_\alpha = \Delta u_\alpha^{ad} + \Delta u_\alpha^{sl}$
  - with the adhesive component defined by a linear relationship (ad)

$$\Delta u_\alpha^{ad} = -\frac{1}{k_T}\Delta p_\alpha\,, \tag{1}$$

  - and the slipping component (sl) defined by the slip rule

$$\dot{u}_\alpha^{sl} = -\dot{\gamma}\frac{\partial \Psi}{\partial p_\alpha}\,, \qquad \Delta u_\alpha^{sl} \approx -\Delta\gamma\frac{\partial \Psi}{\partial p_\alpha}\,, \tag{2}$$

where S_{IJ} is the stress at the contact point, and n_J is the outward normal to the contact surface at the contact point, the tangential displacement in local contact coordinates is denoted by u_α, $\alpha = T_1, T_2$, k_T is the tangential contact stiffness, γ is an unknown function giving the magnitude of slip.

The slip rule plays a similar role in friction to the flow rule in plasticity. The slip potential Ψ is a function of the stress vector, and the derivatives of which give the direction of slipping. In addition a slip criterion Φ is defined to determine the state of friction,

$$\begin{aligned} \Phi \le 0 \;&\Rightarrow\; \text{adhesive state},\\ \Phi > 0 \;&\Rightarrow\; \text{slipping state}. \end{aligned} \tag{3}$$

Further, there exists the following conditions on the slipping/sticking states,

$$\begin{aligned} \text{sticking} \;&\Rightarrow\; \Psi < 0 \;\text{ and }\; \dot{\gamma} = 0,\\ \text{slipping} \;&\Rightarrow\; \Psi = 0 \;\text{ and }\; \dot{\gamma} > 0. \end{aligned} \tag{4}$$

The following particular forms of Ψ and Φ are proposed for the three models considered:

1. the isotropic Coulomb friction

$$\begin{aligned} \Psi(p_\alpha) &= \sqrt{p_\alpha p_\alpha}\,, \\ \Phi(p_\alpha\,, p_{\mathrm{N}}) &= \sqrt{p_\alpha p_\alpha} - \mu p_{\mathrm{N}}\,, \end{aligned} \tag{5}$$

where μ is the coefficient of friction, which may depend on internal parameters such as wear, work-hardening, etc,

2. the WVS model

$$\begin{aligned} \Psi(p_\alpha) &= \sqrt{p_\alpha p_\alpha}\,, \\ \Phi(p_\alpha\,, p_{\mathrm{N}}) &= \sqrt{p_\alpha p_\alpha} - \alpha p_{\mathrm{N}}^{\nu} + \beta p_{\mathrm{N}}\,, \end{aligned} \tag{6}$$

where α, ν and β are the parameters of the model, usually constant, but which may depend on internal parameters such as wear, work-hardening, etc,

3. the work-hardening (WH) model given in de Souza Neto, et al. [8]

$$\begin{aligned} \Psi(p_\alpha) &= \sqrt{p_\alpha p_\alpha}\,, \\ \Phi(p_\alpha\,, p_{\mathrm{N}}, \omega) &= \sqrt{p_\alpha p_\alpha} - \mu(\omega) p_{\mathrm{N}}\,, \end{aligned} \tag{7}$$

where the coefficient of friction $\mu(\omega)$ is now a function of the density of frictional work ω, which is the internal variable of this model,

$$\dot{\omega} = -p_\alpha \dot{u}_\alpha^{\mathrm{sl}}; \qquad \Delta\omega \approx -p_\alpha \Delta u_\alpha^{\mathrm{sl}}\,. \tag{8}$$

A predictor-corrector algorithm is used to calculate the frictional stress and slip over a single timestep. The algorithm for the AC model is given in Fig. 2. Given the current contact pressure

(i) Input: the current increment displacement and pressure

$$\Delta u_\alpha{}^{(n+1)},\ p_{\mathrm{N}}{}^{(n+1)}$$

(ii) Calculate:

Elastic predictor $\qquad p_\alpha^{\mathrm{el}(n+1)} \leftarrow \left(p_\alpha{}^{(n)} - k_{\mathrm{T}} \Delta u_\alpha{}^{(n+1)}\right)$

Slip function $\qquad \Phi \leftarrow \left(\sqrt{p_\beta^{\mathrm{el}(n+1)} p_\beta^{\mathrm{el}(n+1)}} - \mu p_{\mathrm{N}}{}^{(n+1)}\right)$

(iii) Evaluate contact sub-regions:

If $\Phi \le 0$ then adhesion region

set $\quad p_\alpha{}^{(n+1)} \leftarrow p_\alpha^{\mathrm{el}(n+1)}$

Else slipping region

set $\quad p_\alpha{}^{(n+1)} \leftarrow \left[\mu p_{\mathrm{N}}{}^{(n+1)} \left(p_\alpha^{\mathrm{el}(n+1)} \Big/ \sqrt{p_\beta^{\mathrm{el}(n+1)} p_\beta^{\mathrm{el}(n+1)}}\right)\right]$

solve for $\Delta\gamma$: $\quad \sqrt{p_\beta^{\mathrm{el}(n+1)} p_\beta^{\mathrm{el}(n+1)}} - k_{\mathrm{T}} \Delta\gamma - \mu p_{\mathrm{N}}{}^{(n+1)} = 0$

set $\quad \Delta u_\alpha^{\mathrm{sl}(n+1)} \leftarrow -\Delta\gamma \left(p_\alpha^{\mathrm{el}(n+1)} \Big/ \sqrt{p_\beta^{\mathrm{el}(n+1)} p_\beta^{\mathrm{el}(n+1)}}\right)$

Fig. 2. Algorithm for AC friction model over the interval $[t_n\,, t_{n+1}]$

(i) Inpùt: the current increment displacement and pressure

$\Delta u_\alpha{}^{(n+1)}$, $p_N{}^{(n+1)}$

(ii) Calculate:

Elastic predictor $p_\alpha^{el(n+1)} \leftarrow \left(p_\alpha{}^{(n)} - k_T \Delta u_\alpha{}^{(n+1)}\right)$

Slip function $\Phi \leftarrow \left(\sqrt{p_\beta^{el(n+1)} p_\beta^{el(n+1)}} - \alpha\left[p_N{}^{(n+1)}\right]^\nu - \beta p_N{}^{(n+1)}\right)$

(iii) Evaluate contact sub-regions:

If $\Phi \leq 0$ then: adhesion

set $p_\alpha{}^{(n+1)} \leftarrow p_\alpha^{el(n+1)}$

Else: slipping

set $p_\alpha{}^{(n+1)} \leftarrow \left[\left(\alpha\{p_N{}^{(n+1)}\}^\nu + \beta p_N{}^{(n+1)}\right)\left(p_\alpha^{el(n+1)} \Big/ \sqrt{p_\beta^{el(n+1)} p_\beta^{el(n+1)}}\right)\right]$

solve for $\Delta\gamma$: $\sqrt{p_\beta^{el(n+1)} p_\beta^{el(n+1)}} - k_T \Delta\gamma - \alpha\left(p_N{}^{(n+1)}\right)^\nu - \beta p_N{}^{(n+1)} = 0$

set $\Delta u_\alpha^{sl(n+1)} \leftarrow -\Delta\gamma\left(p_\alpha^{el(n+1)} \Big/ \sqrt{p_\beta^{el(n+1)} p_\beta^{el(n+1)}}\right)$

Fig. 3. Algorithm for WVS friction model over the interval $[t_n\,,\, t_{n+1}]$

(i) Input: the current increment displacement and pressure

$\Delta u_\alpha{}^{(n+1)}$, $p_N{}^{(n+1)}$

(ii) Calculate:

Elastic predictor $p_\alpha^{el(n+1)} \leftarrow \left(p_\alpha{}^{(n)} - k_T \Delta u_\alpha{}^{(n+1)}\right)$

Slip function $\Phi \leftarrow \left(\sqrt{p_\beta^{el(n+1)} p_\beta^{el(n+1)}} - \mu(\omega^{(n)}) p_N{}^{(n+1)}\right)$

(iii) Evaluate contact sub-regions:

If $\Phi \leq 0$ then: adhesion

set $p_\alpha{}^{(n+1)} \leftarrow p_\alpha^{el(n+1)}$

Else: slipping

solve for $\Delta\gamma$ and $\omega^{(n+1)}$: $0 = \sqrt{p_\beta^{el(n+1)} p_\beta^{el(n+1)}} - k_T \Delta\gamma - \mu(\omega^{(n+1)}) p_N{}^{(n+1)}$

$$0 = \omega^{(n+1)} - \omega^{(n)} - \mu(\omega^{(n+1)}) p_N{}^{(n+1)} \Delta\gamma$$

set $p_\alpha{}^{(n+1)} \leftarrow \mu(\omega^{(n+1)}) p_N \left(p_\alpha^{el(n+1)} \Big/ \sqrt{p_\beta^{el(n+1)} p_\beta^{el(n+1)}}\right)$

set $\Delta u_\alpha^{sl(n+1)} \leftarrow -\Delta\gamma\left(p_\alpha^{el(n+1)} \Big/ \sqrt{p_\beta^{el(n+1)} p_\beta^{el(n+1)}}\right)$

Fig. 4. Algorithm for WH friction model over the interval $[t_n\,,\, t_{n+1}]$

$p_N{}^{(n+1)}$ and the increment of contact displacement $\Delta u_\alpha{}^{(n+1)}$ at step t_{n+1}, the algorithm provides the frictional stress $p_\alpha{}^{(n+1)}$ and the slip increment $\Delta u_\alpha^{sl(n+1)}$ at step t_{n+1} using the values at the previous step t_n. Firstly the elastic predictor stress is found, then the slip criterion is calculated to determine the state of friction. The frictional stress is exactly the elastic predictor stress for the adhesive state. The frictional stress is set to the limiting stress μp_N, where the direction is along the elastic predictor, for the slipping state. Also the slip contribution is calculated. In a FEM program it is also necessary to provide the derivatives of the frictional stress p_α with respect to the contact presssure p_N and the sliding displacement u_α needed for the Newton-Raphson algorithm. Expressions for $\partial p_\alpha/\partial p_N$ and $\partial p_\alpha/\partial u_\beta$ can be found from consistent linearisation of the frictional constitutive equations.

Figure 3 gives the algorithm for the WVS model. It consists of identical steps to the AC algorithm except for the change in expressions involving μ.

Figure 4 shows the algorithm for the work-hardening friction model. The only difference between this and the AC model is the use of the frictional work internal variable ω. This is changed only when slipping occurs, and must be calculated during the slipping stage of step (iii) of the algorithm.

3. Formulation of the Deep-Drawing Problem

The deep-drawing problem is formulated in the total Lagrangian framework with the following equations:

- equation of motion

$$(S_{KL}\delta_{LI} + S_{KL}u_{L,I})_{,K} + \rho_0 f_I = \rho_0 t_I\,, \tag{9}$$

  - second Piola–Kirchhoff stress tensor S_{KL},
  - displacement u_I,
  - body forces $\rho_0 t_I$,
  - inertia forces $\rho_0 f_I$,

- the elastic-plastic constitutive equation

$$\dot{S}_{KL} = \mathbf{L}^{EP}_{KLMN}\dot{E}_{MN}\,, \tag{10}$$

  - $\mathbf{L}^{EP}_{KLMN}$, the representation of constitutive operator transforming strain rate to stress rate and reflecting elastic and plastic material parameters, also known as the elastic-plastic hyper-operator,
  - Green-Lagrange strain tensor $E_{IJ} = \frac{1}{2}(u_{I,J} + u_{J,I} + u_{K,I}u_{K,J})$.

In the deep-drawing simulation the point on the blank directly under the centre of the punch is the fixed point that is required to ensure the existance and uniqueness of the numerical solution. This point moves down with the punch, and is then fixed during each step of the solution calculation. The mathematical necessity of the fixed point boundary condition is essential otherwise the solution for the displacement is not unique. The existence and uniqueness of solution of frictional contact problems were broadly discussed by Demkowicz et al. [2].

The conditions for the deep-drawing finite element simulation are the following:

- boundary conditions on the surface ${}^t\Gamma_U$ where the boundary displacement is given $u_I = \phi_I(\mathbf{X}, \xi)$, for particles $\mathbf{X} \in {}^t\Gamma_U$ and time $\xi \in (t_n\,,\, t_{n+1})$.
- fixed point of the blank $\mathcal{P} \in {}^t\Gamma$ where $\phi(\mathbf{X}, \xi) = 0$, $\partial\phi(\mathbf{X}, \xi)/\partial\mathbf{N} = 0$, $(\mathbf{X}, \xi) \in {}^t\Gamma_U \times (t_n\,,\, t_{n+1})$,
- boundary conditions on surface ${}^t\Gamma_F$ where force G_I is prescribed $(S_{KL}\delta_{LI} + S_{KL}u_{L,I})N_K = G_I$,

- boundary conditions on the contact surface ${}^t\Gamma_C$ with applied friction T_{T_i}, $S_{IJ}N_J - S_{JK}N_JN_KN_I = T_{T_i}$, $i = 1, 2$,
- initial conditions $u_I(\mathbf{X}, 0) = 0$ and $\dot{u}_I(\mathbf{X}, 0) = 0$.

4. Deep-drawing simulation

The simulation of the deep-drawing process is conducted for a three-dimensional prismatic square-cup. The FE model of prismatic-cup deep-drawing [7] consists of three tools: punch, die and blankholder, shown in Fig. 5, and a single workpiece: the blank. The dimensions for the tools and material parameters for this simulation are taken from the benchmark chosen for the NUMISHEET'93 conference.

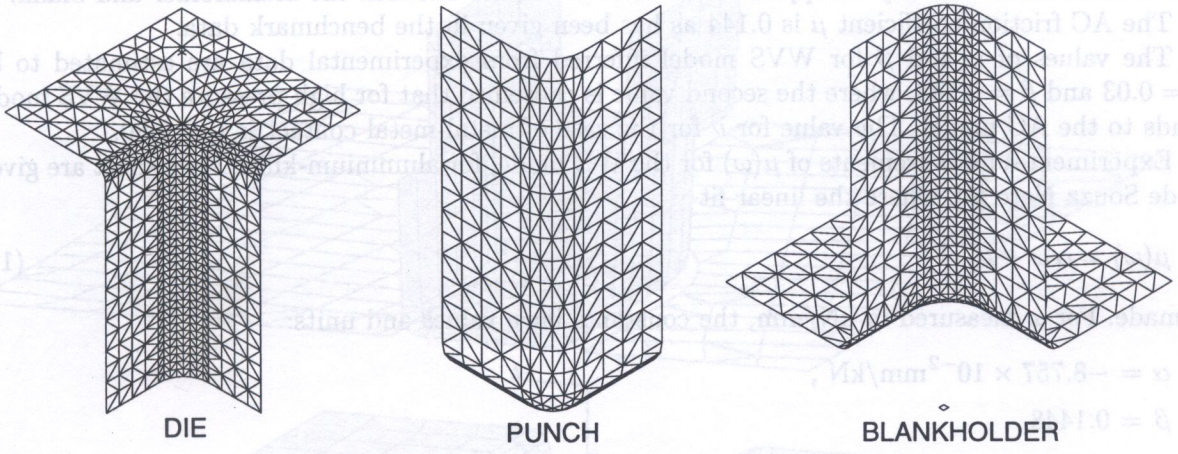

Fig. 5. The die, punch, and blankholder used in the deep-drawing simulation (only one-quarter shown)

The dimensions for the square-cup deep-drawing tools are:

Tool piece	Dimensions		Rounding radii
	internal (mm)	external (mm)	(mm)
die	66 × 66	170 × 170	12
blankholder	84 × 84	170 × 170	12
punch		70 × 70	10

The clearance between the die and the punch is 2 mm, and between the punch and the blankholder is 7 mm. The mesh for the three tools are shown in Fig. 5. The workpiece is 150 × 150 mm in size with a thickness of 0.78 mm and is made of mild sheet steel with the following material properties:

Young's modulus	206 GPa,
Poisson's ratio	0.30,
Yield stress	$\sigma = 565.32\,(\varepsilon_p + 0.007117)^{0.2589}$,
Coefficient of friction	0.144.

Only one quarter of the blank and tools are modelled for this FE simulation because there exist two axes of symmetry. Two thousand and five hundred shell elements are used to model the quarter of the blank with a uniform mesh of 50 × 50 elements. The tools are modelled using rigid Bézier surfaces.

The stepping procedure for this FE simulation is as follows:

(1) Place blank on die; place blankholder above die.

(2) Move punch down by 0.01 mm.

(3) Fix punch in place; apply blankholder force.

(4) Move punch down to full stroke.

Step (1) sets up the tools and blank in the correct positions without the blankholder force. In step (2) the punch is moved down slightly to establish contact between the punch and blank, and also between the blankholder and blank. In step (3) the blankholder force is applied to the blankholder. The punch is then moved down to the full stroke in step (4). Step (2) is necessary to establish contact between the tools and the blank, before the blankholder force can be applied. The blankholder force can only be applied once there is contact between the blankholder and blank.

The AC friction coefficient μ is 0.144 as has been given in the benchmark data.

The values of α and β for WVS model inferred from experimental data are estimated to be $\alpha = 0.03$ and $\beta = 0.144$, where the second value is chosen so that for high pressure the WVS model tends to the AC model. The value for ν for the case of metal-metal contact is $\nu = 0.80$.

Experimental measurements of $\mu(\omega)$ for the WH model for aluminium-killed steel sheet are given in de Souza Neto [8], where the linear fit

$$\mu(\omega) = \alpha\omega + \beta \tag{11}$$

is made. For ω measured in kN/mm, the constants have values and units:

$$\alpha = -8.757 \times 10^{-2}\text{mm/kN}\,,$$

$$\beta = 0.1448.$$

This fit for the function $\mu(\omega)$ actually represents a "work-softening", as the decrease in the value for μ as ω increases reflects the smoothing of the surface of the blank when the asperities are flattened by sliding.

5. S-Rail simulation

The S-rail simulation is taken from the NUMISHEET'96 conference benchmark and consists of a similar set of tools as shown in Fig. 6. There is no simple symmetry and the entire set is used in the simulation. Two meshes are used: a medium mesh and a fine mesh shown in Fig. 7 at the full displacement.

The S-rail forming process is modelled with a double-action simulation: the first step closes the blankholders; the second step moves the punch to its full stroke. This is illustrated in Fig. 8.

The blank has thickness of 1.0 mm and is made of mild sheet steel with the following material properties:

Young's modulus	206 GPa,
Poisson's ratio	0.30,
Yield stress	$\sigma = 526\,(\varepsilon_p + 0.015)^{0.239}$,
Coefficient of friction	0.11.

The AC friction coefficient μ is 0.11 as has been given in the benchmark data.

The values of α and β for WVS model inferred from experimental data are estimated to be $\alpha = 0.03$ and $\beta = 0.11$, where the second value is chosen so that for high pressure the WVS model tends to the AC model. The value for ν for the case of metal-metal contact is $\nu = 0.80$.

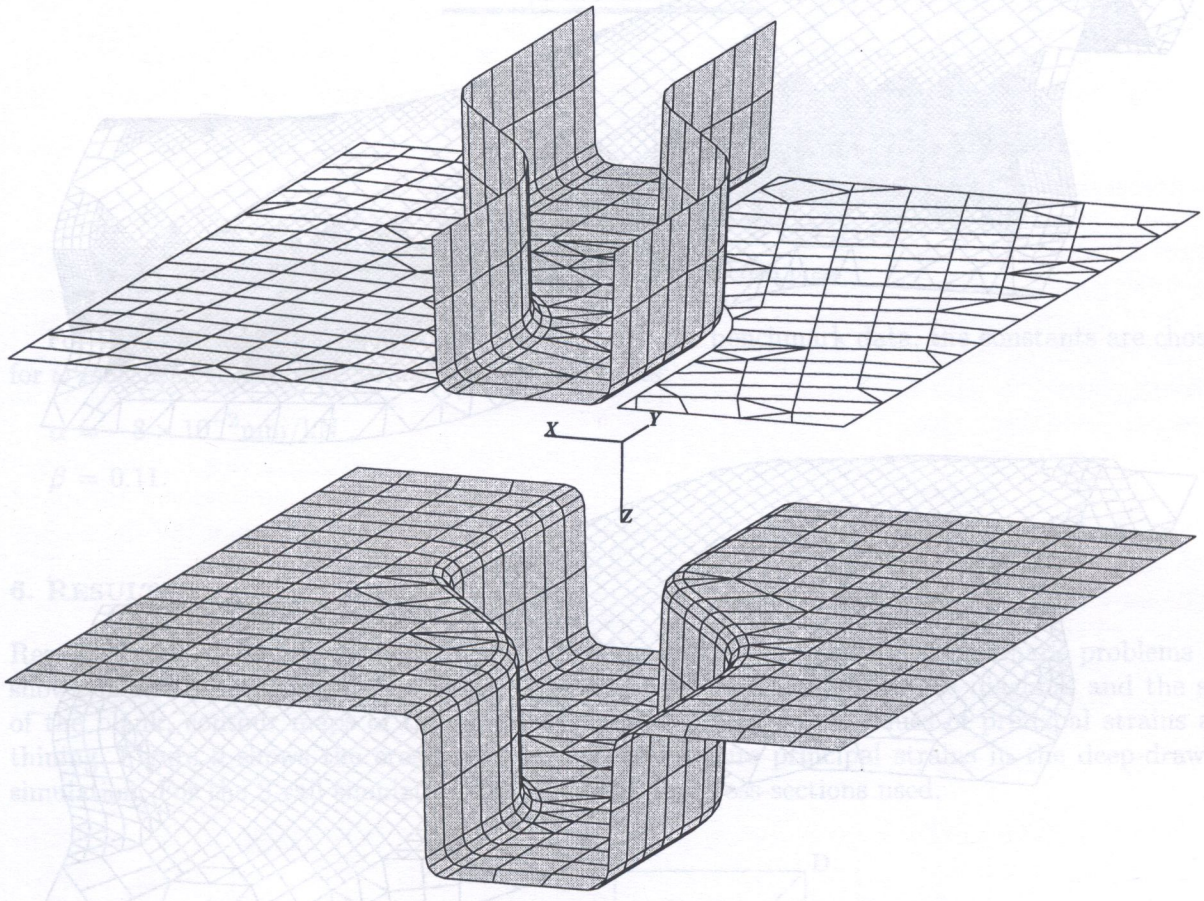

Fig. 6. The die, punch, and blankholder used in the S-rail simulation

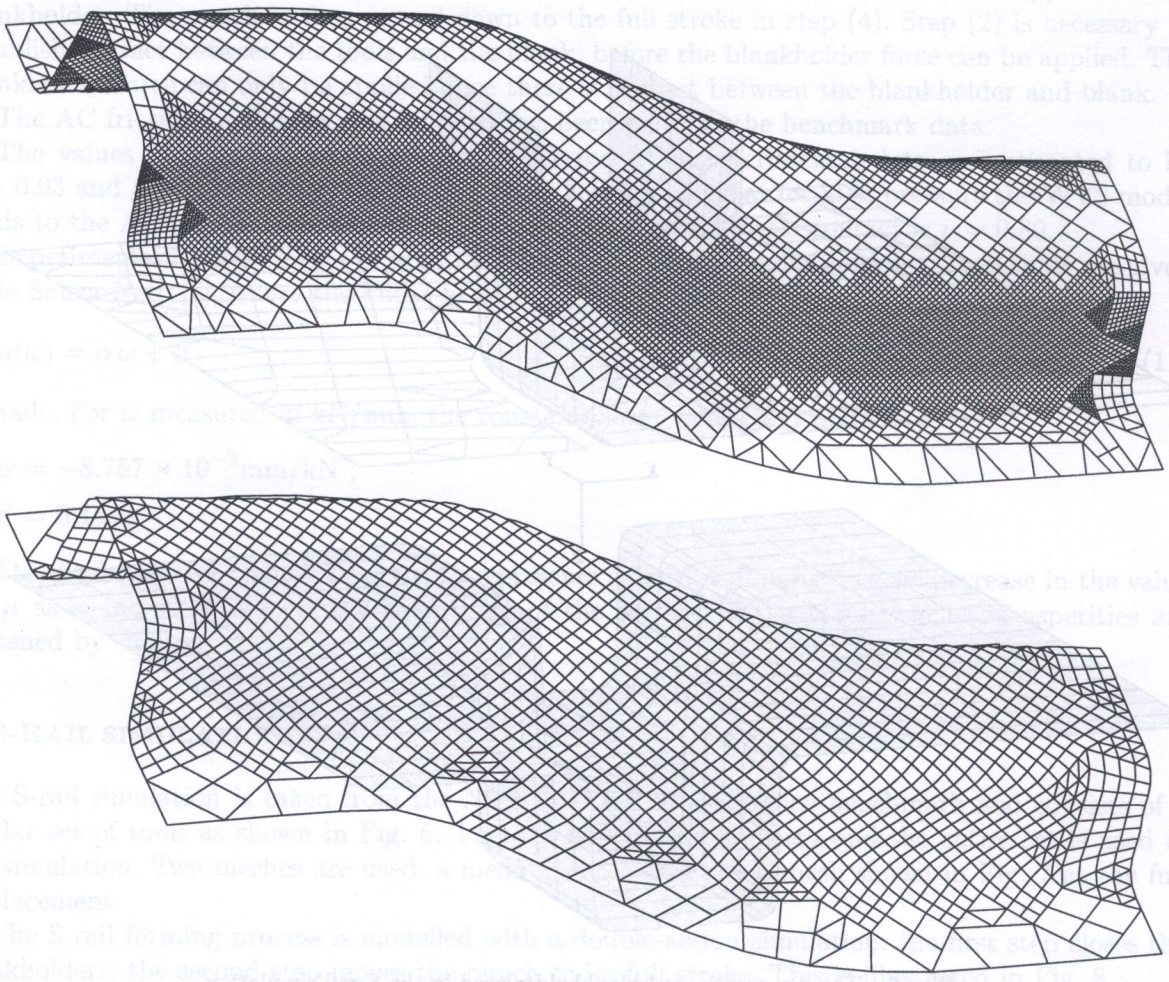

Fig. 7. Comparison of the coarse and fine meshes showing the final deformed shape of the work piece

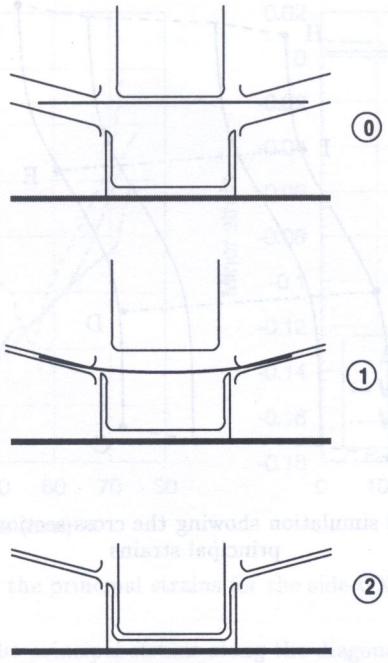

Fig. 8. Steps of the double-action press

For the WH model, to ensure compatibility with the benchmark data, the constants are chosen, for ω measured in kN/mm, to have values and units:

$\alpha = -8 \times 10^{-2}$mm/kN ,

$\beta = 0.11$.

6. Results

Results obtained for the square-cup deep-drawing and S-rail stamping benchmark problems are shown in the form of plots of principal strains vs. distance along both the diagonal and the side of the blank, contour maps of thinning, and tables with extremal values of principal strains and thining. Figure 9 shows the cross-sections used to measure principal strains in the deep-drawing simulation. For the S-rail simulation Fig. 10 shows the cross-sections used.

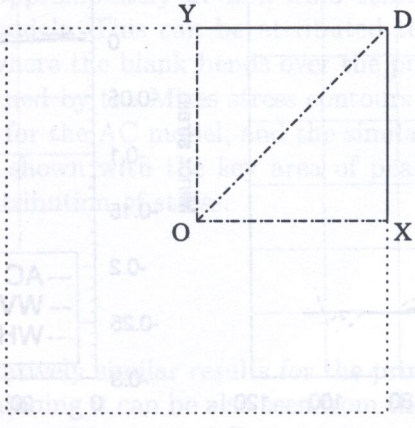

Fig. 9. Schematic of the deep-drawing simulation showing the cross-sections OX and OD used for measuring principal strains. As shown, only one-quarter of the blank is modelled with suitable boundary conditions applied along OY and OX to accommodate the symmetry

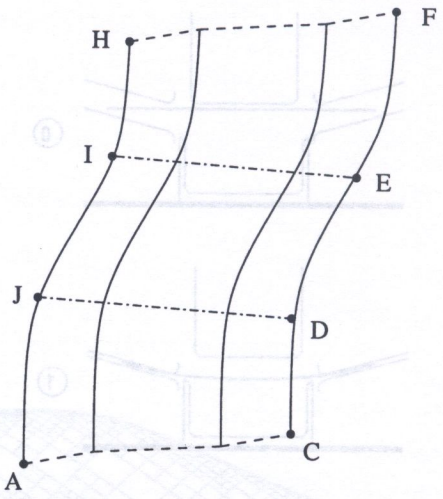

Fig. 10. Schematic of the S-rail simulation showing the cross-sections EI and DJ used for measuring principal strains

6.1. Deep-drawing

Figures 11 and 12 illustrates that the AC model has the largest strain values, which is due to this model using a constant value for the coefficient of friction and not taking into account the variation of μ from pressure and wear as in the case of the WVS and WH models, respectively. The WH and AC results are similar because the WH model is a modification of the AC model with work-hardening included. The WVS results are different in shape from the AC and WH models as its non-linear term dominates.

These features are confirmed in Tables 1 and 2 which show the maxima and minima of the strains. Along the diagonal OD the WVS and WH models have smaller extrema than the AC model as shown in Table 1 and Fig. 11. The WVS model's maximum is 47% smaller than the AC model, which indicates that the nonlinear term, $\alpha p_{\mathrm{N}}^{\nu}$, of the WVS model contributes significantly. The lower values of the extrema of the WH model indicate that slipping work has smoothed the surface and reduced the friction stresses.

Along the side OX it is found that the major strain maxima for the WVS and WH models differ by a small amount as shown in Table 2 and Fig. 12. However, for the WVS model the minor strain

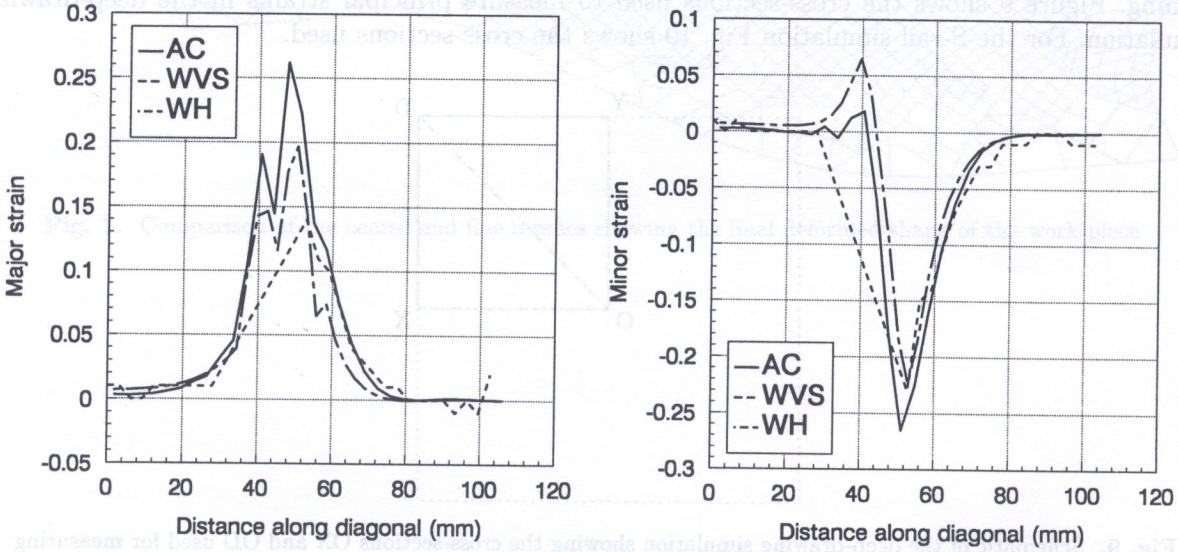

Fig. 11. Graphs showing the principal strains for the diagonal of the deep-drawing blank

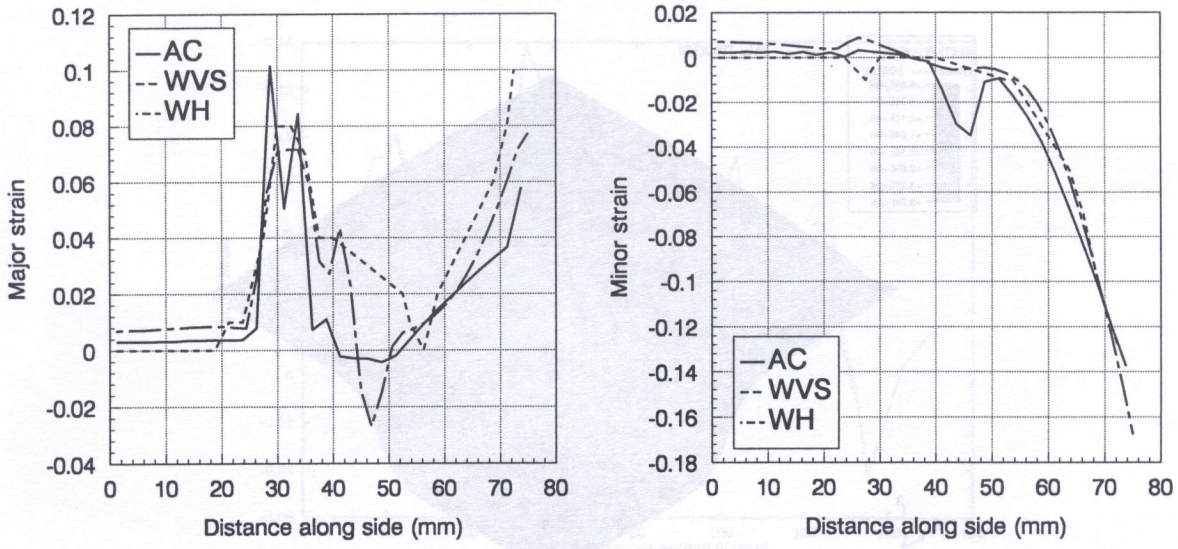

Fig. 12. Graphs showing the principal strains for the side OX of the deep-drawing blank

Table 1. Extreme values for the principal strains along the diagonal of the deep-drawing workpiece

Friction model	Along diagonal OD			
	major strain		minor strain	
	maxima	% resp. to AC	minima	% resp. to AC
AC	0.263	100	−0.262	100
WVS	0.140	53	−0.225	86
WH	0.197	75	−0.220	84

Table 2. Extreme values for the principal strains along the side of the deep-drawing workpiece

Friction model	Along side OX			
	major strain		minor strain at punch edge	
	maxima	% resp. to AC	extrema	% resp. to AC
AC	0.1013	100	0.0033	100
WVS	0.0800	79	−0.0100	303
WH	0.0713	70	0.0083	251

extrema near the punch edge (approximately 27 mm from centre) is a minima compared to the maxima for the AC and WH models. This can be attributed to the nonlinear term dominating under the high pressure region where the blank bends over the punch.

These observations are confirmed by the Mises stress contours in Fig. 13. They show the overal higher values of the Mises stress for the AC model, and the similar distribution for the WH model. The lower WVS values are also shown with the key area of peak values at the corner appearing smaller in size showing lower distribution of stress.

6.2. S-Rail

The medium mesh reveals qualitatively similar results for the principal strains and thinning across cross-section IE in Fig. 14. For thinning it can be also seen from the smooth contour plots in Fig. 15. The peaks are mostly at the same position with differences occuring in value. The relatively coarse mesh shown in Fig. 7 reveals the likely reason: the larger elements tend to smooth out the results and offer lower resolution. The differences in the finer mesh results of Fig. 16 are more dramatic.

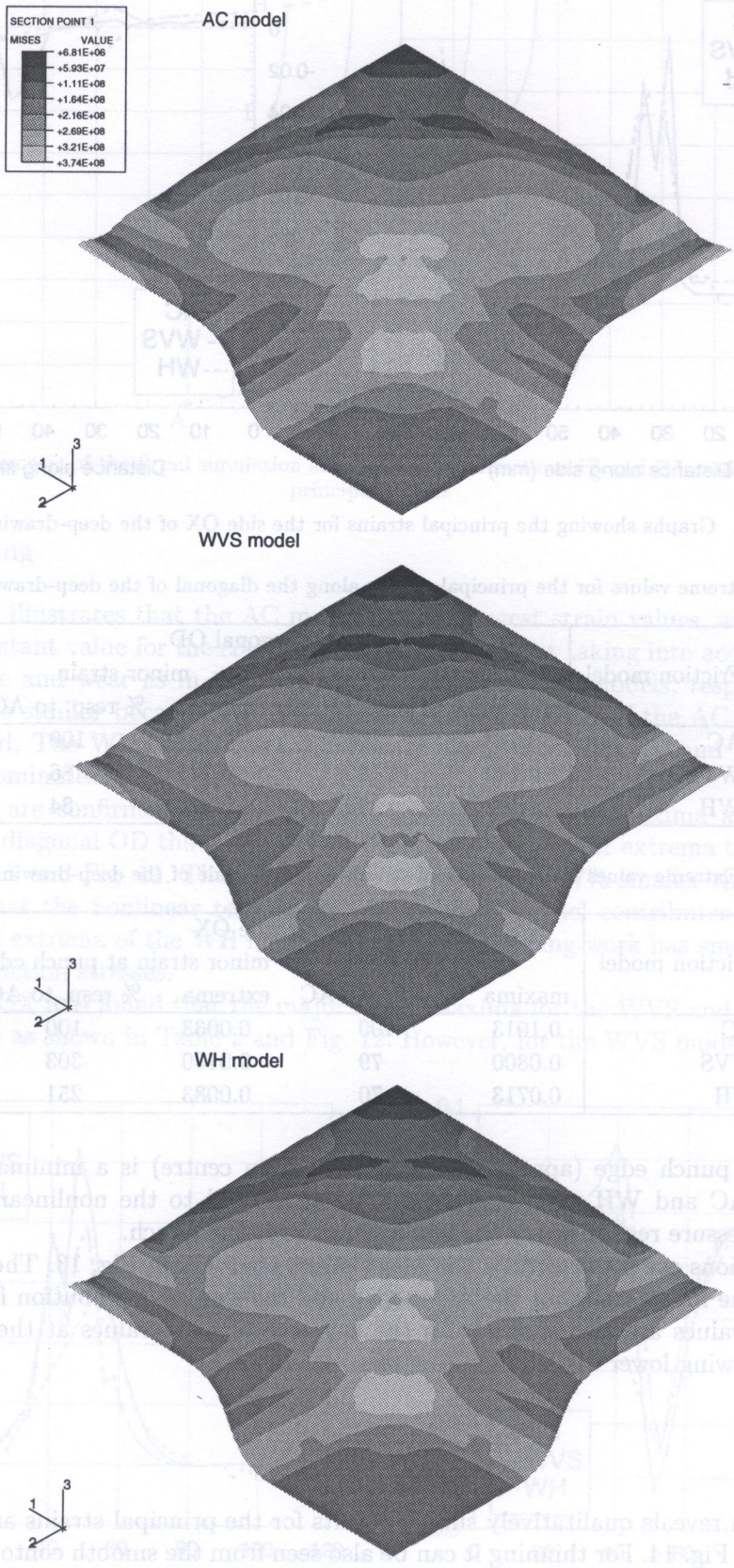

Fig. 13. Contour plots of Mises stress distribution for the deep-drawing simulation

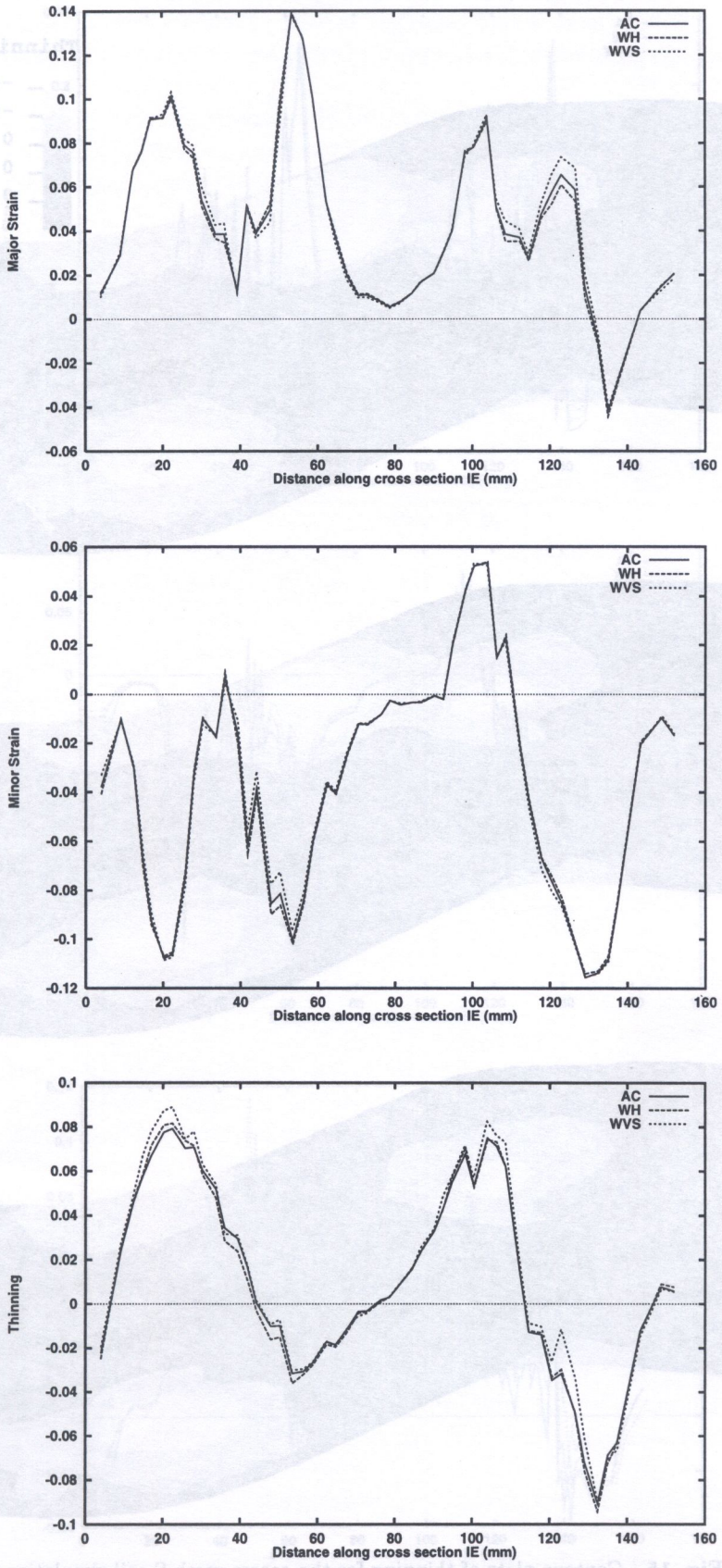

Fig. 14. Graphs showing the principal strains and thinning for the section IE of the S-rail blank with coarse mesh

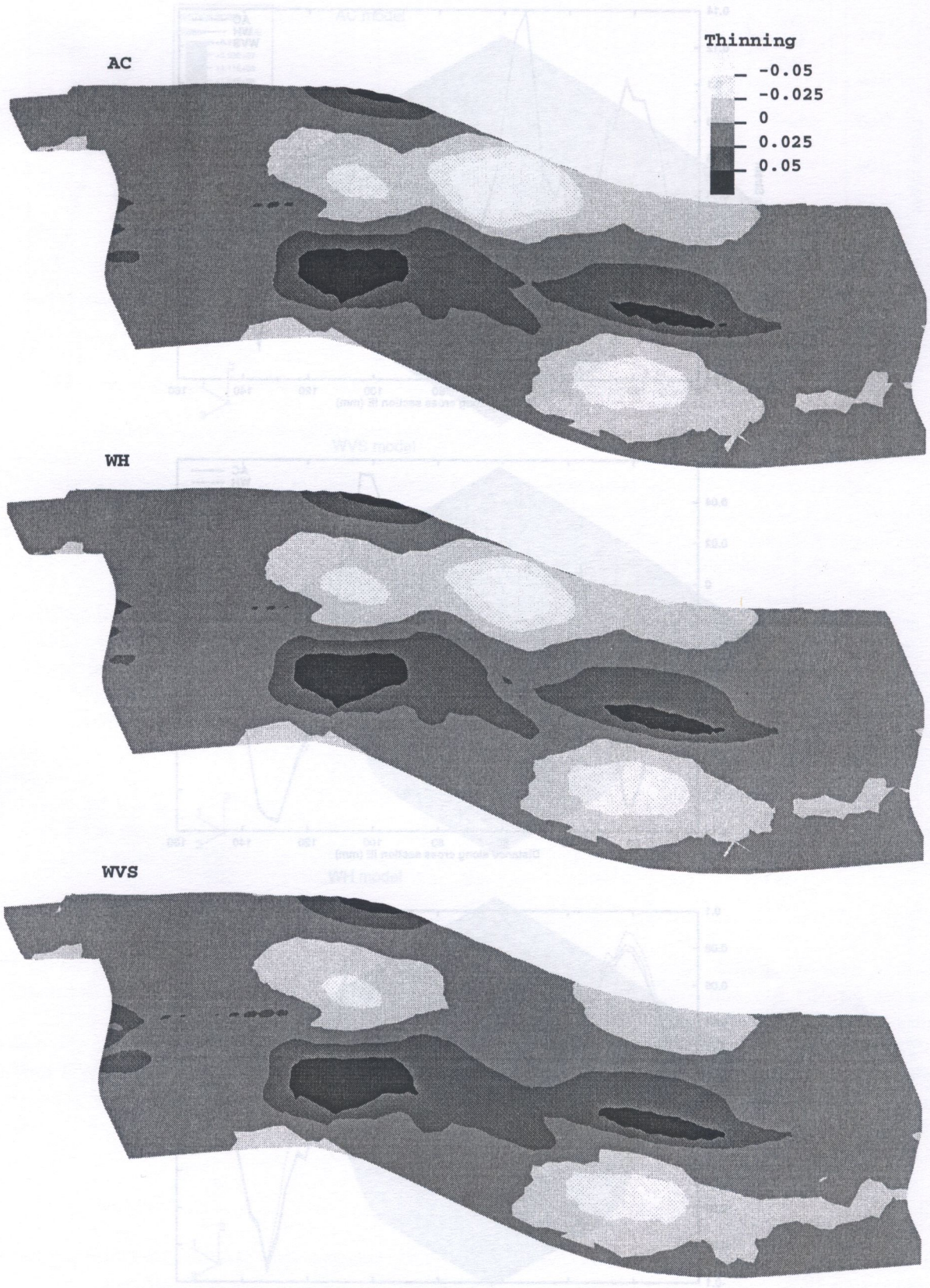

Fig. 15. Contour plots of thinning for the coarse mesh S-rail simulation

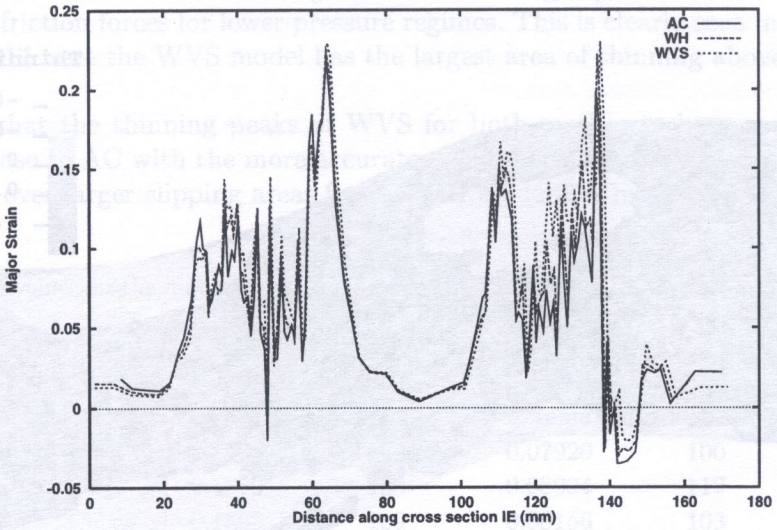

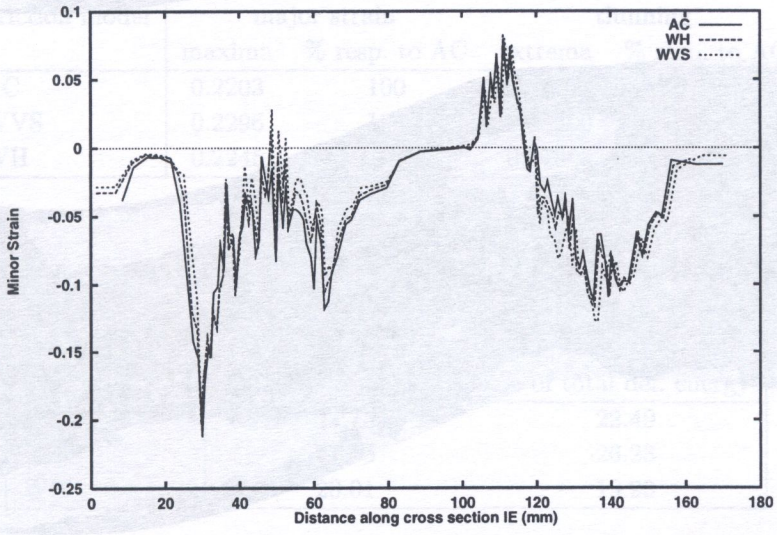

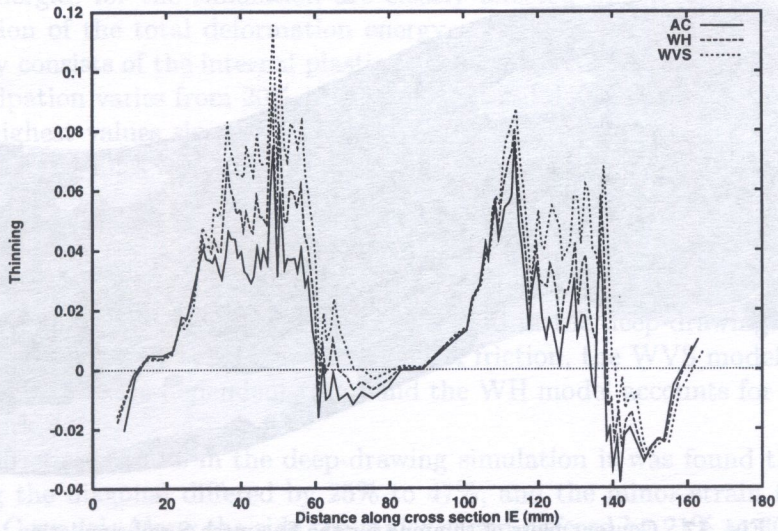

Fig. 16. Graphs showing the principal strains and thinning for the section IE of the S-rail blank with fine mesh

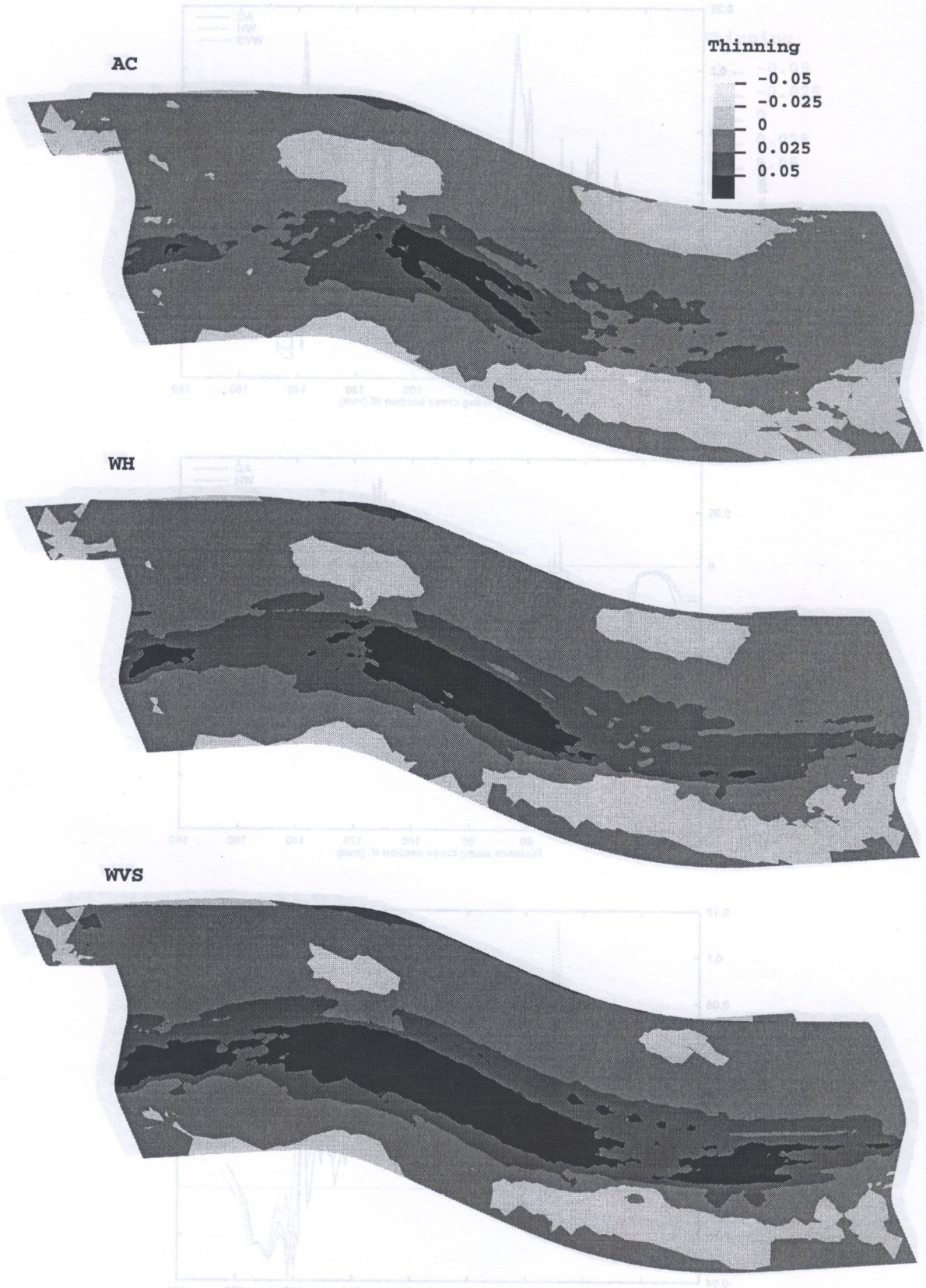

Fig. 17. Contour plots of thinning for the fine mesh S-rail simulation

The greatest distinction in the the thinning curves where larger peaks for the WVS model are a result of its higher friction forces for lower pressure regimes. This is clearly seen in the contour maps of thinning in Fig. 17 were the WVS model has the largest area of thinning above 5% in the wall of the S-rail.

Table 3 shows that the thinning peaks of WVS for both meshes to be some 11%–12% higher than AC. WH is close to AC with the more accurate result for the fine mesh showing it lower. Here the reduction in μ over larger slipping areas for the WH model has made a significant contribution to the result.

Table 3. Extreme values for the major principal strain and thinning along the line EI of the S-rail workpiece

Friction model	Coarse Mesh major strain maxima	% resp. to AC	thinning extrema	% resp. to AC
AC	0.1278	100	0.07920	100
WVS	0.1379	108	0.08904	112
WH	0.1393	109	0.08156	103
Friction model	**Fine Mesh major strain maxima**	**% resp. to AC**	**thinning extrema**	**% resp. to AC**
AC	0.2203	100	0.07502	100
WVS	0.2296	104	0.08300	111
WH	0.2245	102	0.07063	94

Table 4. Proportion of energy devoted to frictional dissipation with respect to internal energy of the S-rail simulation

Friction model	coarse mesh % of total def. energy	fine mesh % of total def. energy
AC	24.75	22.49
WVS	27.75	26.23
WH	20.01	19.93

Globally, the energies for the simulation are clearly affected by the different models. Table 4 shows the proportion of the total deformation energy accounted for by frictional work. The total deformation energy consists of the internal plastic work and the contact sliding work. Table 4 shows that frictional dissipation varies from 20% to 28% of the total deformation energy. As expected the WVS model has highest values since the frictional forces are higher for lower pressure areas. The WH model shows lower values than AC as the lower μ value requires less frictional work.

7. Conclusions

Three friction models of different characteristics were used in the deep-drawing and S-rail simulations. The AC model has a single constant coefficient of friction, the WVS model has three parameters with a nonlinear pressure-dependent term, and the WH model accounts for wear proportional to the frictional work.

Using different friction models in the deep-drawing simulation it was found that the results for major strain along the diagonal differed by 25% to 47%, and the minor strain from 14% to 16%, compared to the AC model. Along the side the major strain differed by 21% to 30%, and the minor strain at the punch edge differed by 150% to 200%, compared to the AC model. These values have sufficient variation to indicate that more accurate models of friction are needed for this simulation.

WH generally gives similar results to AC, which is related to the history of deformation of the blank. This is because the value of μ for the AC model represents an 'average' of the function $\mu(\omega)$ for the WH model. The WVS model uses only the current state of pressure and does not consider the history of the surface deformation.

In the S-rail simulation results were presented for two mesh sizes. The less fine mesh showed little difference between the friction models, however, the finer mesh results showed differences almost a large as for deep-drawing. This indicates that large element sizes tend to reduce the contribution of friction and hence are less accurate.

The energy results show that the three friction models contribute significantly to the final result. Friction is thus an important part of the simulation and the need for more accurate friction models is crucial in the S-rail simulation.

For the two typical metal forming simulations it has been shown that friction plays a crucial role and that the different friction models influence the result as much as 25%. The accuracy of metal forming simulations thus depends as much on a more accurate, more realistic, friction model as on a sufficiently fine mesh.

References

[1] A. Curnier. A theory of friction. *Int. J. Solids Structures*, **20**: 637–647, 1984.

[2] L. Demkowiwicz, J.T. Oden. On same existence and uniqueness results in contact problems with non-local friction. *Nonlinear Anal. Theory Meth. Appl.*, **10**: 1075–1093, 1984.

[3] T.J.R. Hughes, R.L. Taylor, J.L. Sackman, A. Curnier, W. Kanoknukulchai. A finite element method for a class of contact-impact problems. *Comp. Meth. Appl. Mech. Engng.*, **8**: 249–276, 1976.

[4] R. Michałowski, Z. Mróz. Associated and nonassociated sliding rules in contact friction problems. *Arch. Mech.*, **30**: 259–276, 1978.

[5] J. Rońda, K.W. Colville. Comparison of friction models for deep-drawing. *GAMM-Mitteilungen*, **18**: 39–59, 1995.

[6] J. Rońda, K.W. Colville, Z. Mróz. Co-rotational friction model for metal forming. In: J.K. Lee, G.L. Kinzel, R.H. Wagoner (eds.), *Proceedings of NUMISHEET '96*, Dearborn, Michigan, pp. 47–54, 1996.

[7] J. Rońda, C.D. Mercer, A.S. Bothma, G.J. Oliver, K.W. Colville. Simulation of square-cup deep-drawing with various friction and material models. *Journal of Materials Processing Technology*, **50**: 92–104, 1995.

[8] E.A. de Souza Neto, K. Hashimoto, D. Perić, D.R.J. Owen. A phenomenological model for frictional contact accounting for wear effects. *Phil. Trans. R. Soc. London*, **A354**: 819–843, 1996.

[9] P. Wriggers, T. vu Van, E. Stein. Finite element formulation of large deformation impact-contact problems with friction. *Computers and Structures*, **37**: 319–331, 1990.